Effects of Precursor and Support Variation in the Genesis of Uranium Oxide Catalysts for CO Oxidation and Selective Reduction of NO: Synthesis and Characterization

Tom Campbell,[†,‡] Mark A. Newton,*[,†,§] Vicky Boyd,[||] Darren F. Lee,[||] and John Evans*[,†]

School of Chemistry, University of Southampton, Highfield, Southampton SO17 1BJ, United Kingdom, and Nuclear Sciences and Technology Services, British Nuclear Fuels Plc, Springfields, Preston, Lancashire PR4 0XJ, United Kingdom

Received: June 21, 2004; In Final Form: October 4, 2004

A range of uranium oxide-based catalysts, derived from $UO_2(NO_3)_2 \cdot 6H_2O$ and UCl_4 precursors, and supported on γ-Al_2O_3, SiO_2 and mesoporous H_1SiO_2, have been synthesized and then characterized using the following methods: isothermal nitrogen adsorption/desorption measurements, diffuse reflectance infrared spectroscopy (DRIFTS), gas titration of surface hydroxyl groups using Grignard reagents, U L_{III} extended X-ray absorption fine structure (EXAFS), powder X-ray diffraction (PXRD), and thermogravimetric and differential thermal analysis. Brij76-templated H_1SiO_2 mesoporous silicas are found to be essentially stable under flowing oxygen after 16 h at 1073 K. At temperatures above this, however, extensive structural collapse, together with extensive dehydroxylation, ensues. Titration of the accessible hydroxyl group concentrations shows that in these materials the density of OH groups is considerably lower than in their amorphous counterparts. The adsorption of uranyl nitrate onto these dispersants results in a supported, and partially dehydrated, phase of the parent molecule with little obvious structural distortion; however, the adsorption of UCl_4 leads to a complex adstructure which may best be described as $U(O)_2Cl_2$. The subsequent formation of the uranium oxide phase, nominally active for the oxidation of CO and selective reduction of NO (generally accepted to be U_3O_8), is found to be a considerable function of both the precursor and support system employed. Calcination of such systems to 1073 K results in extensive extrusion of the supported uranium phase from mesoporous supports, resulting in the formation of very large orthorhombic U_3O_8 domains. PXRD, however, shows that on amorphous SiO_2 and γ-Al_2O_3 similar treatment results in the formation of a hexagonal phase of U_3O_8. The formation of U_3O_8 is found to be promoted in mesoporous systems and by the presence of Cl in the catalyst make up. Some evidence is also found that suggests that a persistence of Cl limits the growth of U_3O_8 domains.

Introduction

Uranium displays a profoundly rich and complex oxide chemistry with an almost continuous range of reduced phases having been observed from U(VI)O_3 to U(II)O along with a number of polymorphs.[1] Though complicated, this range of reducibility does, however, provide the potential for an equally diverse redox chemistry that may be utilized to facilitate catalytic processes. Uranium-based systems, often in conjunction with a second metal oxide, have been shown to catalyze a variety of partial and total oxidation processes: uranium−molybdenum oxides have been reported as active for isobutene conversion to acrolein,[2] and uranium−antimony has found industrial application in the partial oxidation of propene to acrolein and acrylonitrile.[3] The formation of highly defective (oxygen deficient) phases, crucial for the attainment of effective redox couples in such systems, is emphasized by the behavior of Bi_2UO_6 in the oxidative demethylation of toluene.[4] A high selectivity for this reaction is only achieved in the absence of gaseous oxygen; indeed this material can lose 50% of its lattice oxygen without substantial structural modification.[5]

The use of both bulk and supported uranium oxides in total oxidation reactions for pollution control has gathered interest, particularly in light of the work of Hutchings et al.[6] who showed that U_3O_8 is an extremely effective catalyst for the complete oxidation of a range of chlorinated organic compounds to carbon oxides, HCl, and water.

The use of similar systems for oxidation reactions involving CO as reductant can, however, be traced back to the work of Nozaki et al.[7,8] in the early 1970s. They found that systems based upon a nominal U_3O_8 phase were active for the catalytic oxidation of CO by O_2 and that using an alumina support promoted this conversion. SiO_2 carriers were however found to suppress performance. This same group also showed that bulk U_3O_8 also catalyzes the selective reduction of NO to N_2 by CO.[9] Further, this research indicated that the use of a dispersant greatly enhances activity and that such enhancements showed a significant support dependency. Most interestingly in the current case it was found that the use of SiO_2, compared to Al_2O_3, again suppressed catalytic performance,[9] and that differing supports destabilized the uranyl nitrate precursor employed, in favor of the formation of U_3O_8, in the order $TiO_2 > SiO_2 > Al_2O_3$.[10]

This work has been recently extended by Wells et al.[11] They found that high-temperature calcination (1073 K) of a uranyl

* To whom correspondence should be addressed. E-mails: newton@esrf.fr; je@soton.ac.uk.

† University of Southampton.

‡ Present address: Johnson Matthey Plc, Royston, Hertfordshire, United Kingdom.

§ Present address: European Synchrotron Radiation Facility, ESRF, 6 rue Jules Horowitz, BP 220, 38043 Grenoble Cedex 9, France.

|| British Nuclear Fuels Plc.

10.1021/jp0404394 CCC: $30.25
Published on Web 01/27/2005

nitrate precursor supported (at 30 wt % loading) on γ-Al_2O_3 led to the formation of catalysts that showed a considerably reduced reaction light off and enhanced activity for NO removal. At low space velocities (ca. 2300 h^{-1}) the net activity for NO removal in these systems was found to be comparable to that shown by typical Pt/γ-Al_2O_3 systems. Moreover, the formation of N_2O was greatly suppressed in the uranium-based systems, especially in the temperature region around light off where this is a considerable contributor to the net product distribution obtained over the Pt-based catalysts.

Experimental Section

1. Synthesis of H_1SiO_2 and Characterization of Support Materials. H_1SiO_2 was prepared by the method due to Attard et al.[12] One mass equivalent of Brij76 surfactant was dissolved in two mass equivalents of $(CH_3O)_4Si$. One mass equivalent of dilute HCl was then added to yield pH 1.3. The resulting mixture was then held in vacuo at 310 K for 30 min to remove CH_3OH produced by the hydrolysis of the $(CH_3O)_4Si$. The resulting gel was then left to condense for 1−2 days to yield a colorless glassy solid. This was then heated to 743 K under 20 mL min^{-1} N_2 for 4 h before the flow was switched to 20 mL min^{-1} oxygen for 8 h in order to remove the template.

The H_1SiO_2 samples were characterized using X-ray diffraction (XRD), isothermal nitrogen adsorption/desorption (to yield total (BET) surface area and pore size distribution via the Dollimore−Heal method[13]), diffuse reflectance infrared absorption spectroscopy, and gas titration methods. Amorphous SiO_2 (ES70, Grace) and γ-Al_2O_3 (Degussa) were used as supplied.

2. Synthesis and Characterization of Uranium Tetrachloride Precursor. The uranyl nitrate hexahydrate $(UO_2(NO_3)_2 \cdot 6H_2O$, Strem) was used as supplied.

Uranium tetrachloride was synthesized by the method due to Herman and Shuttle[14] using uranium(IV) oxide. A 10 g amount of UO_2 and 25 cm^3 of hexachloropropene were placed in a three-neck flask, fitted with a condenser and N_2 bubbler, and slowly heated to 333 K to induce a highly exothermic reaction. At this point the flask was cooled in ice water to prevent the sample temperature exceeding 373 K. After this initial reaction had subsided, the mixture was refluxed at 431 K for 6 h. The resulting red mixture was then filtered using a Schlenk apparatus and the green uranium tetrachloride collected and washed with dry dichloromethane. The uranium tetrachloride sample was characterized using diffuse reflectance UV−vis/near-IR spectroscopy and XRD with reference to the literature.[15−17]

3. Deposition of Precursors and Characterization of Supported Materials. For all supports, uranium precursors were wet impregnated: $UO_2(NO_3)_2 \cdot 6H_2O$ was dissolved in distilled water and then added dropwise to the support material and stirred for 2 h. The solvent was then removed under vacuum before drying at 373 K under vacuum for 12 h. The procedure for supporting uranium tetrachloride was identical; however, tetrahydrofuran was used as the solvent rather than water.

4. Isothermal Nitrogen Adsorption/Desorption Measurements. Nitrogen adsorption measurements were collected at 77 K, using a Micromeritics GEMINI III 2375 surface area analyzer. Typically, a sample charge of 30 mg was used for measurement.

5. Gas Titration of Hydroxyl Groups. A precisely measured mass of previously calcined (at temperatures ranging from 743 to 1173 K) silica was placed in an evacuable flask and flushed with N_2. Butyl ether (5 cm^3) was added to the flask and then degassed by repeated freeze−pump−thaw cycles. The pressure of the system was then measured prior to the introduction of methylmagnesium bromide (5 cm^3 of 1.0 M solution in butyl ether). The system was then left to return to its original temperature for 2 h before the final pressure was recorded. The net pressure change was then used to calculate the number of hydroxyl groups present in the sample with the implicit assumption that the Grignard reacts only with surface hydroxyl species to generate 1 mol of CH_4/(surface OH group).

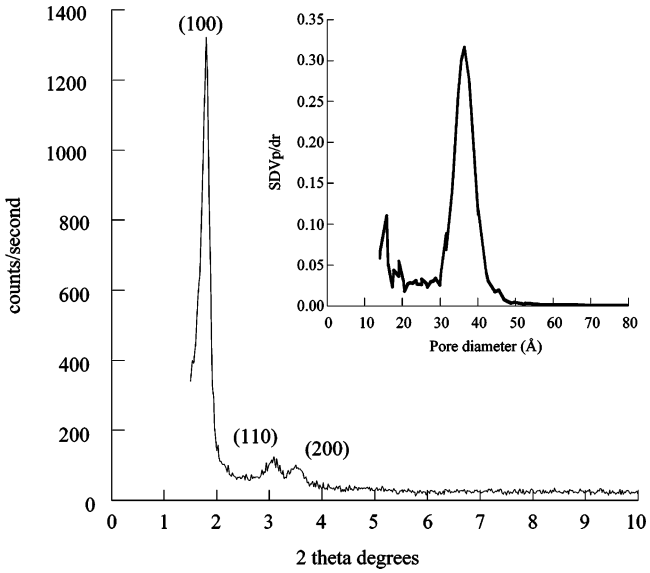

Figure 1. PXRD pattern derived from Brij76-templated H_1SiO_2 after treatment under flowing N_2 (20 mL min^{-1}, 743 K, 4 h) followed by calcination under O_2 (20 mL min^{-1}, 743 K, 8 h). The insert shows the associated Dollimore−Heal pore size distribution derived from N_2 adsorption/desorption meansurements.

6. PXRD. Powder X-ray diffraction (PXRD) measurements were carried out at room temperature using a Siemens $\theta-2\theta$ D5000 diffractometer fitted with a Cu anode. Detection of the diffracted beam was made using a scintillation counter. In situ variable-temperature XRD measurements were made using a Philips Xpert MPD diffractometer, again using Cu Kα in conjunction with an Anton Parr XRK cell. It should be noted that whereas the former experimental setup was capable of resolving orthorhombic U_3O_8 from its hexagonal polymorph, the latter in situ measurements lacked the required angular resolution to do so. As such, the in situ measurements can only index the appearance of U_3O_8 with no specification as to the polymorphs present.

7. U L_{III} EXAFS Measurements. These were performed at stations 9.2 of the Synchrotron Radiation Source (Daresbury Laboratory) using a double-crystal Si (220) monochromator. Both supported and bulk uranium samples were diluted to ca. 10 wt % uranium using dry boron nitride. X-ray absorption spectra were collected in transmission mode. Subsequent data reduction was performed using PAXAS[18] and full curved wave, multiple scattering analysis in EXCURV98.[19]

Results

1. Characterization and Stability of H_1SiO_2 Supports. Figure 1 shows low-angle PXRD derived from Brij76-templated mesoporous silica after treatment in N_2 and O_2 at 743 K. The insert shows the associate Dollimore−Heal pore size distribution derived from isothermal N_2 adsorption experiments. Three diffraction peaks are clearly seen, indicative of a high level of order in the system with pores ca. 38 Å in diameter. The average interpore wall thickness is estimated to be 17−18 Å given that

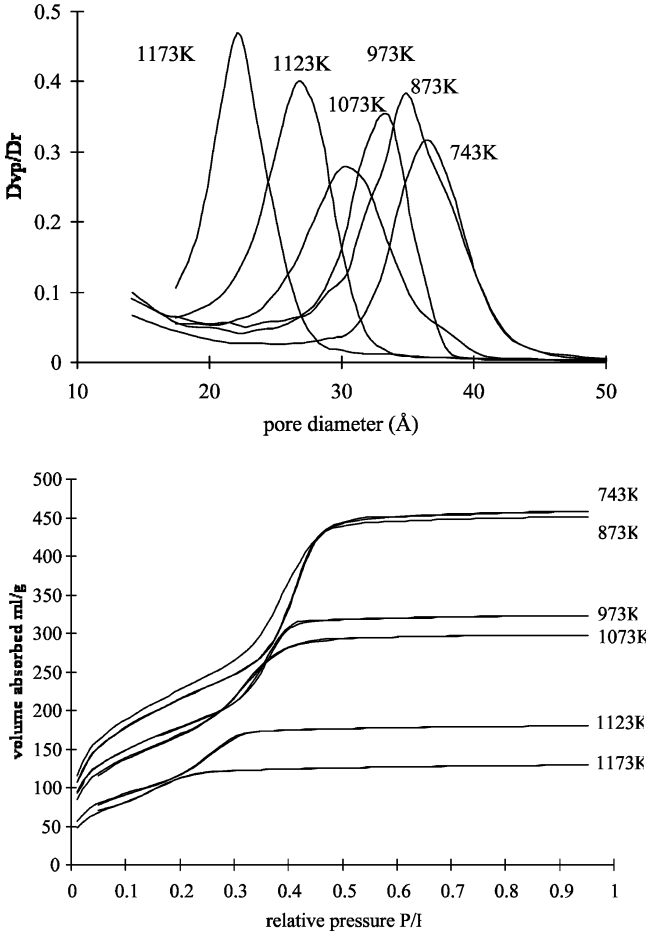

Figure 2. (a, top) Dollimore−Heal pore size distributions derived from Brij76-templated H_1SiO_2 after calcination in O_2 (20 mL min^{-1}) for 16 h at the temperatures indicated. (b, bottom) Isothermal N_2 adsorption/desorption curves derived from Brij76-templated H_1SiO_2 after calcination under O_2 (20 mL min^{-1}) for 16 h at the temperatures indicated.

the interpore wall thickness − pore diameter = $d_{100}/(\cos 30°)$. Figure 2a shows Dollimore−Heal pore size distributions derived from H_1SiO_2 samples, calcined in flowing (20 mL min^{-1}) O_2 for 16 h at temperatures from 843 to 1173 K. Figure 2b shows the corresponding isothermal nitrogen adsorption/desorption traces, and Figure 3 the results derived from ex situ PXRD data, obtained after calcination to a variety of temperatures, regarding the variation of d_{100}.

These measurements point to these materials largely retaining their mesoporous architecture to temperatures in excess of 1000 K, though a gradual shrinkage of the average pore size from ca. 38 to 30 Å within this temperature range is observed. Above ca. 1073 K a collapse of the tertiary structure of the silica occurs such that by 1223 K (not shown) no (100) reflection is observed.

Figure 4a presents corresponding ex situ DRIFTS experiments performed after calcination at the temperatures indicated. Figure 4b brings together the derived variations of total surface area and total silanol concentrations (from Grignard titration experiments) as a function of temperature for the H_1SiO_2 and SiO_2 samples.

It is clear from these data that dehydroxylation, surface area loss, and pore shrinkage go hand in hand. However, these materials are essentially dehydroxylated by 1073 K, whereas significant losses of surface area are not observed until after this temperature is reached. Further, the titration experiments show that the silanol densities achievable in these mesoporous systems are only at most ca. 1−2 OH nm^{-2} compared to the

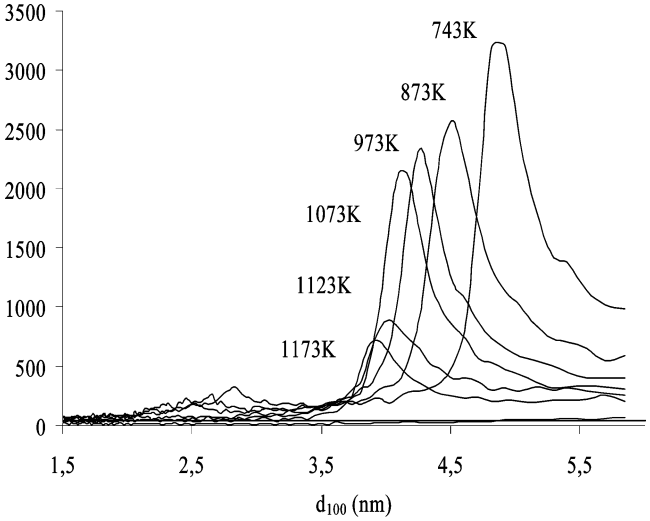

Figure 3. Variation of d_{100} (nm), from ex situ PXRD measurements, for the Brij76-templated materials as a function of calcination (in O_2 (20 mL min^{-1}) for 16 h) temperature.

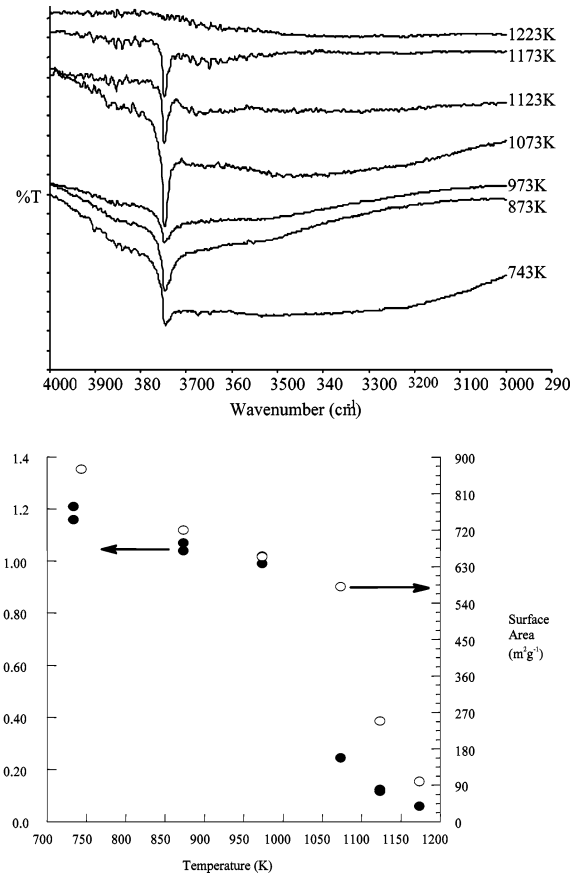

Figure 4. (a, top) Ex situ DRIFTS spectra derived from Brij76-templated H_1SiO_2 samples after calcination (under O_2 (20 mLmin^{-1}) for 16 h) at the temperatures indicated. (b, bottom) Total accessible hydroxyl concentrations, derived from Grignard titration experiments, along with (BET) surface areas obtained from the Brij76-templated H_1SiO_2 materials as a function of calcination temperature.

maximal OH concentrations obtainable on amorphous silicas. For instance the same pretreatments and titration experiments conducted upon ES70 yield up to ca. 5.7 OH nm^{-2} after dehydroxylation at 473 K and 2.4 OH nm^{-2} after dehydroxylation at 1073 K.[20] The density of islolated silanols in the H_1SiO_2 materials is therefore approximately half that attainable in amorphous analogues.

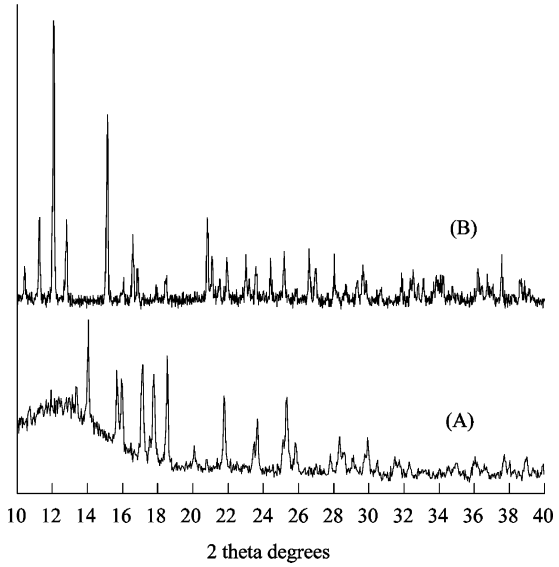

Figure 5. PXRD patterns derived from as-deposited $U(O)_2(NO_3)_2 \cdot 6H_2O/H_1SiO_2$ (A) and $U^{IV}Cl_4/H_1SiO_2$ (B) deposited materials (30 wt % uranium) after drying at 373 K for 12 h.

2. Characterization of Uranium-Deposited Materials. Figure 5 shows PXRD patterns derived from dried uranium-loaded H_1SiO_2 samples (30 wt % uranium) for uranyl nitrate and UCl_4 precursors. Though not shown here, similar results are obtained from PXRD investigation of uranium-loaded amorphous SiO_2 and γ-Al_2O_3 samples. The phase present after drying of the uranyl nitrate hexahydrate deposited material (Figure 5a) is identified as being uranyl nitrate dihydrate,[21] showing that low-temperature drying of the catalysts has precipitated a degree of dehydration of the hexahydrate. The diffraction pattern derived from the H_1SiO_2-supported UCl_4-derived system is far more complex (Figure 5b) and not easily reconcilable with any known bulk examples of uranium chloride or oxychloride; some similarity does, however, exist between this pattern and that derived from neutron diffraction for orthorhombic oxide dichloride.[22]

U L_{III} edge XAS measurements made on the uranyl nitrate derived material confirmed the conclusions of the PXRD experiments, in that the EXAFS derived is indistinguishable from that derived from the pure uranyl nitrate. The U L_{III} edge k^3 EXAFS spectrum, Fourier transform, and fits due to theoretical analysis in EXCURV98, derived from the supported UCl_4/H_1SiO_2 material, are shown in Figure 6a,b. The structural and statistical parameters derived from data spectra are given in Table 1, alongside those for bulk UCl_4 (from EXAFS and previous neutron diffraction measurements).[17] The fitting of the UCl_4 is found to be in good accord with previously obtained neutron diffraction data. However, it is clear that, in line with the PXRD measurements shown in Figure 5, there are considerable differences between UCl_4 and the uranium phase that arises from its being supported upon H_1SiO_2 dried at 373 K.

The coordination of oxygen atoms at ca. 2.22 Å is similar to that expected from a single U−O bond[23] derived from a charged oxygen donor,[24] rather than a double-bonded oxygen (axial U═O bonds are usually observed at ca. 1.75 Å with little variation due to differing equatorial ligands).[23] This indicates that this phase is not a U(VI) system. The derived U−Cl distances are similar (2.61 Å compared to 2.63 Å); however, attempts to fit a second Cl shell at ca. 2.8 Å, as would be expected from UCl_4, result in a steep increase in the *R*-factor. In a further difference to that expected from pure UCl_4, uranium shells may be fitted at 3.68 and 4.31 Å. These distances rule out the formation of a tetrahydrofuran adduct being present[25] and strongly point to the presence of a mixture of bridging U−Cl−U and U−O−U bonds being present in this material.

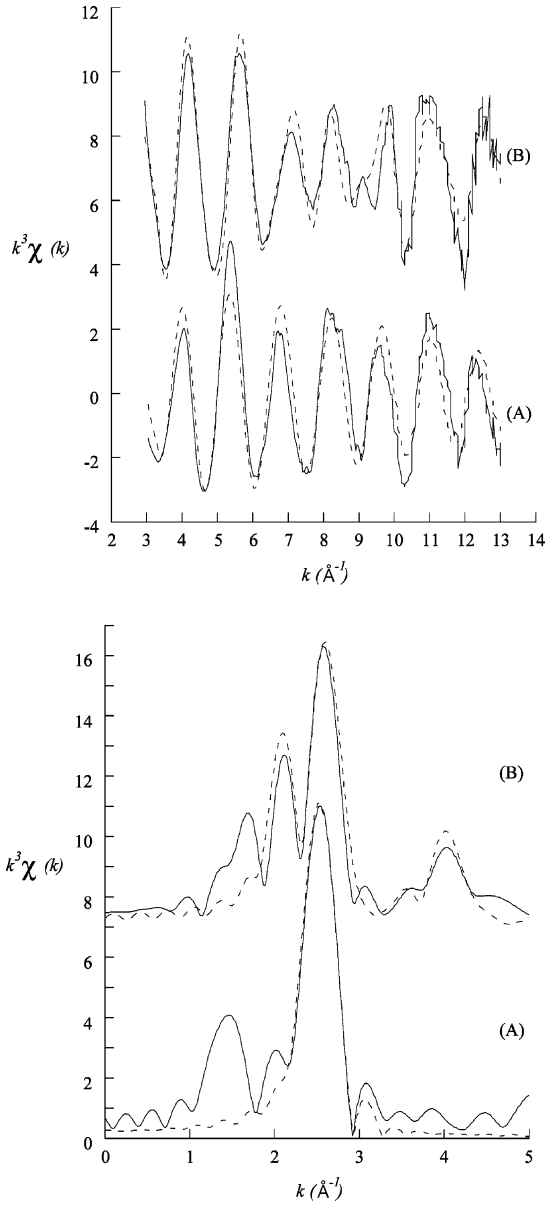

Figure 6. (a, top) k^3-weighted U L_{III} EXAFS, derived from (A) $U^{IV}Cl_4$ and (B) the $U^{IV}Cl_4/H_1SiO_2$ system, after drying and dilution to 10 wt % U in boron nitride. Theoretical fits derived from analysis in EXCURV98 are also shown (dashed lines). (b, bottom) Fourier transforms derived from U L_{III} EXAFS derived from (A) UCl_4 and (B) the UCl_4/H_1SiO_2 system after drying and dilution to 10 wt % U in boron nitride. Theoretical fits derived from analysis in EXCURV98 are also shown (dashed lines).

3. Characterization of Calcined Materials. Figure 7a shows PXRD patterns derived from the calcination of H_1SiO_2-, SiO_2-, and Al_2O_3-supported uranyl nitrate samples after calcination at 1073 K for 3 h under flowing (20 mL min^{-1}) O_2. Figure 7b shows the equivalent PXRD patterns derived from the same treatment of systems where uranium(IV) chloride has replaced uranyl nitrate as the precursor. Also indicated are the particle thicknesses calculated for each case using the Scherrer formula[26] as applied to the U_3O_8 [001] reflection. This reflection is chosen as its shape is polymorph-independent; the other reflections at higher angles split due to the lowering of symmetry between hexagonal and orthorhombic phases of U_3O_8.

TABLE 1: Structural and Statistical Data from Analysis of U L_{III} Edge EXAFS Derived from UCl_4 and 30 wt % UCl_4/H_1SiO_2 after Drying at 373 K[a]

	atom type	coordination no.	bond length (Å)	bond length neutron (Å)[29]	Debye−Waller ($2\sigma^2$/Å^2)	E_F (eV)	*R*-factor (%)
UCl_4	Cl	4.0	2.63(1)	2.634(4)	0.013(2)		
						−7.6	36.14
	Cl	4.0	2.82(2)	2.866(1)	0.028(2)		
	O	2.0(2)	2.22(1)	N/A	0.007(1)		
UCl_4/H_1SiO_2	Cl	3.9(2)	2.61(1)	N/A	0.018(1)		
						−2.3	32.14
	U	2.0(4)	3.68(1)	N/A	0.013(3)		
	U	2.0(5)	4.31(3)	N/A	0.018(4)		

[a] Both samples were diluted to a net 10 wt % U in boron nitride prior to EXAFS measurement.

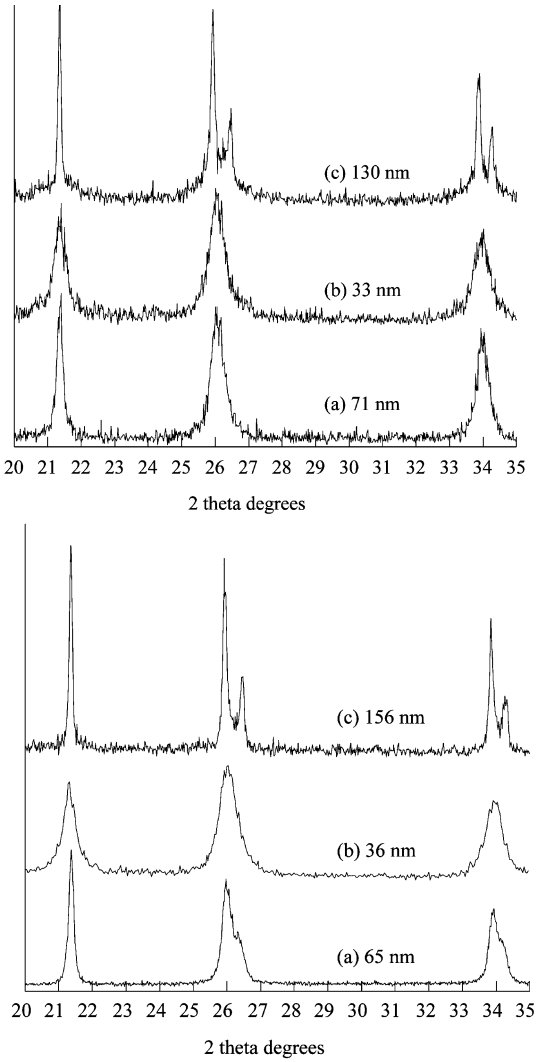

Figure 7. (a, top) PXRD patterns derived from $U(O)_2(NO_3)_2{\cdot}6H_2O$ supported upon (spectrum a) Al_2O_3, (spectrum b) SiO_2, and (spectrum c) H_1SiO_2 after calcination under O_2 (20 mL min^{-1}) for 3 h at 1073 K. (b, bottom) PXRD patterns derived from UCl_4 supported upon (spectrum a) Al_2O_3, (spectrum b) SiO_2, and (spectrum c) H_1SiO_2 after calcination under O_2 (20 mL min^{-1}) for 3 h at 1073 K.

The diffraction patterns for both calcined uranyl nitrate and uranium(IV) chloride system (Figure 7a,b, spectrum c in both cases), supported upon H_1SiO_2, shows the formation of orthorhombic U_3O_8. When SiO_2 and Al_2O_3 are used as supports, U_3O_8 is also formed, but the lack of splitting in the peaks at ca. 26 and 34° 2θ indicates that in these cases the hexagonal form of this oxide predominates. An exception to this general observation, in the systems supported upon amorphous oxides, is the UCl_4/Al_2O_3 case (Figure 7b, spectrum a). In this case an asymmetry in the diffraction features at ca. 26 and 34° 2θ is observed, suggesting the presence of relatively small domains of hexagonal U_3O_8. Application of the Debye−Scherrer formula quantifies the considerable variations in U_3O_8 domain sizes produced in each of the cases investigated. Along with yielding a different polymorph of U_3O_8, the H_1SiO_2-supported systems also produce U_3O_8 domain sizes 3−4 times larger than their amorphous counterparts. Indeed, these U_3O_8 domains are very much larger than the average pore size derived from unloaded systems treated to the same temperature (Figure 2a).

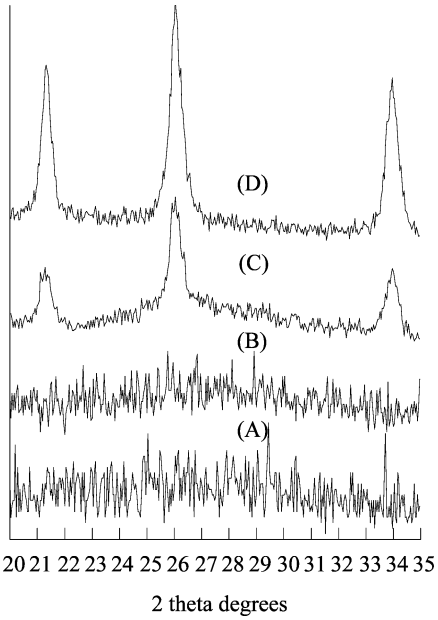

Figure 8. PXRD patterns derived from $U(O)_2(NO_3)_2{\cdot}6H_2O$ and $U^{IV}Cl_4$ samples calcined to 723 K: (A) $U(O)_2(NO_3)_2{\cdot}6H_2O/Al_2O_3$; (B) $U(O)_2(NO_3)_2{\cdot}6H_2O/H_1SiO_2$; (C) $U^{IV}Cl_4/Al_2O_3$; (D) $U^{IV}Cl_4/H_1SiO_2$

Figure 8 shows PXRD derived from these systems after similar treatment to 723 K. At 723 K it is only the chloride-derived samples supported upon the mesoporous silica and the alumina that show evidence for the extensive formation of U_3O_8, and no significant diffraction is observed from any of the nitrate-derived systems. An orange color persists in these latter systems, indicating the persistence of amorphous and weakly diffracting UO_3 phases,[27] as opposed to the olive green of U_3O_8. These data suggest that the presence of Cl in the catalyst promotes the formation of U_3O_8. It is also the case that, relative to the amorphous silica, the use of a mesoporous silica also promotes U_3O_8 formation. However, at 723 K it appears that the U_3O_8 is hexagonal in the H_1SiO_2 just as is found at higher temperatures on the amorphous supports. It would appear therefore that in the mesoporous systems the hexagonal phase forms initially but is replaced by the orthorhombic after calcination to 1073 K.

These effects have been investigated in more detail using in situ PXRD, thermogravimetric (TGA), and differential thermal (DTA) analyses. Figure 9a shows data derived from and in situ

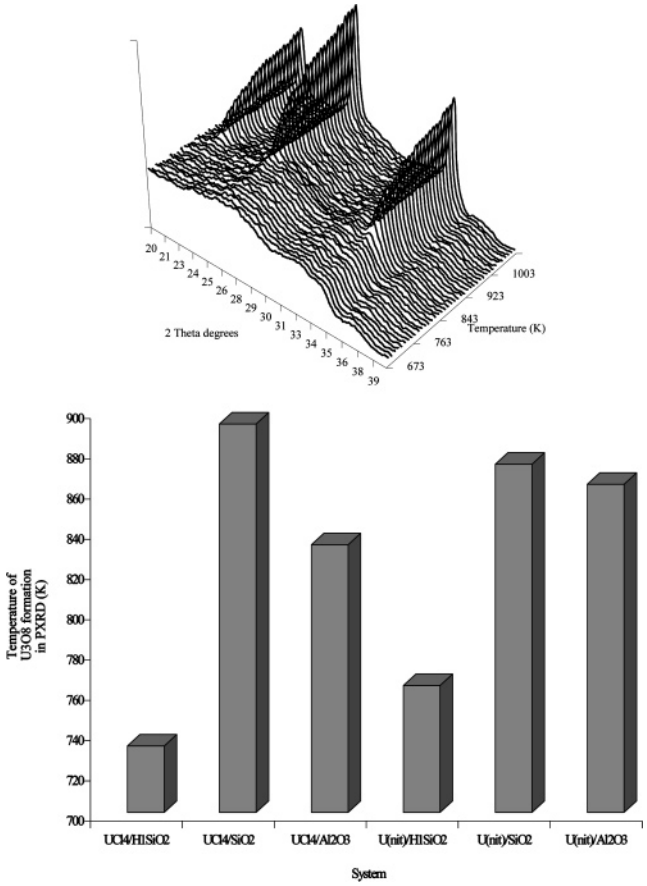

Figure 9. (a, top) Variable-temperature PXRD derived from the calcination of $U^{IV}Cl_4/\gamma$-Al_2O_3 samples in static air showing the development of supported U_3O_8 domains. The data have been smoothed for presentation purposes. (b, bottom) Temperature at which "PXRD visible" U_3O_8 domains become observable during calcination in static air for the range of support/precursor combinations investigated.

temperature programmed PXRD derived under static air. It is clear that by 673 K the original precursor has collapsed to be replaced by some intermediate, noncrystalline, phase, though two very broad peaks can be detected at ca. 27.5 and 33° 2θ. This would be consistent with a poorly ordered cubic or quasi cubic (UO_2 to $UO_{2.37}$) arising from the initial collapse of the supported precursors: this situation is found for all systems studied. This poorly ordered phase then reacts further as the temperature is increased. In the case shown, diffracting U_3O_8 domains are only observed above 830 K. Figure 9b collates the temperature at which such diffraction visible domains appear for the six systems studied.

This verifies, and yields greater detail regarding, the support/precursor dependencies observed in U_3O_8 formation. The precursor-induced differences are relatively small (<30 K). However, a mesoporous silica architecture induces a considerable promotion (by ca. 160 K compared to amorphous SiO_2) of U_3O_8 formation.

TGA and DTA curves obtained during in situ calcination for these systems are shown in Figure 10a (uranyl nitrate-based samples) and Figure 10b (UCl_4-based systems) along with traces derived from the same treatment applied to bulk uranyl nitrate and uranium chloride. The data derived from the pure uranyl nitrate are consistent with a previously described sequence of dehydration events,[28] and, though not shown here, down stream mass spectroscopic analysis during calcination shows that NO losses occur at between 443 and 473 K (minor) and 560 K (major) as gaseous NO and NO_2. Alongside these events water is seen to be sequentially lost in three determinable stages up to ca. 470 K. The major weight loss event (that of NO at 560 K) can clearly be seen to be support-dependent with the H_1SiO_2-supported uranyl nitrate showing this event to occur at approximately the same temperature as that for the bulk case. However, when supported upon amorphous SiO_2 and Al_2O_3, the major weight loss event is promoted by ca. 60 K. Beyond 600 K there is no further significant weight loss, though DTA data show that there are additional (predominantly exothermic) events occurring at higher temperatures (between 700 and 800 K for all systems, and again at $T > 900$ K (for amorphous systems only)) for which there is no corresponding mass loss. The same experiments conducted upon uranium chloride-derived systems show considerable variation between both supported systems and bulk UCl_4, and between the supported materials themselves. Bulk UCl_4 shows three mass loss events. The mass loss for the feature centered around 670 K corresponds to the following conversion:[29]

$$UCl_4 + O_2 \rightarrow UO_2Cl_2 + Cl_2$$

Once supported, decomposition of the parent precursor is greatly promoted. Once again, on-line mass spectrometry shows that the highest temperature events observed in these cases are not associated with Cl loss. Instead these features (occurring at ca. 670 K for the H_1SiO_2 and Al_2O_3 systems, and ca. 640 K in the amorphous silica case) are due to loss of CO_2 derived from the cracking of tetrahydrofuran that has failed to escape the sample in vapor form. In all cases that fragment of the residual solvent that does escape the system intact during these experiments is shown in the TGA by the lowest temperature features observed. Chlorine is progressively lost in each system between these two extreme events.

In the case of the UCl_4/Al_2O_3-derived systems the levels of chlorine retention as a function of calcination temperature were also investigated. Figure 11 shows the results derived for ICP analysis for the Cl retention observed in these cases as a function of calcination temperature systems. Alongside these data, postcalcination, PXRD-derived, U_3O_8 crystallite sizes are also shown. Chlorine is lost progressively up to ca. 870 K. Concomitant with the loss of Cl, U_3O_8 domains appear in PXRD and between 840 and 900 K their size stays within 20−30 Å. Thereafter the U_3O_8 phase steadily grows to yield domains 60−70 Å in thickness by 1073 K.

Discussion

The use of a Brij 76 template and the synthetic approach of Attard et al.[12] for the formation of mesoporous silicas produces high-quality and, importantly, thermally robust materials with initial pore diameters of ca. 30−38 Å (after calcination to temperatures in the range 743−1023 K). Increasing calcination temperature in an oxidizing environment causes an apparent shrinkage in average pore size and gradual loss of surface area until ca. 1073 K. Up to this point all the interrogative measurements applied indicate the large-scale retention of the mesoporous architecture, though the net pore diameter has shrunk to ca. 32 Å with a concomitant loss of ca. 30% of the surface area compared to the as-made material. Above 1073 K a rapid loss of structural integrity is, however, indicated.

Titration of accessible surface OH groups in the mesoporous material indicates that the H_1SiO_2 materials are considerably more hydrophobic than their amorphous counterparts, showing maximal OH densities that are only ca. 50% of that attainable in the amorphous silica used in this study.[20] As with the total

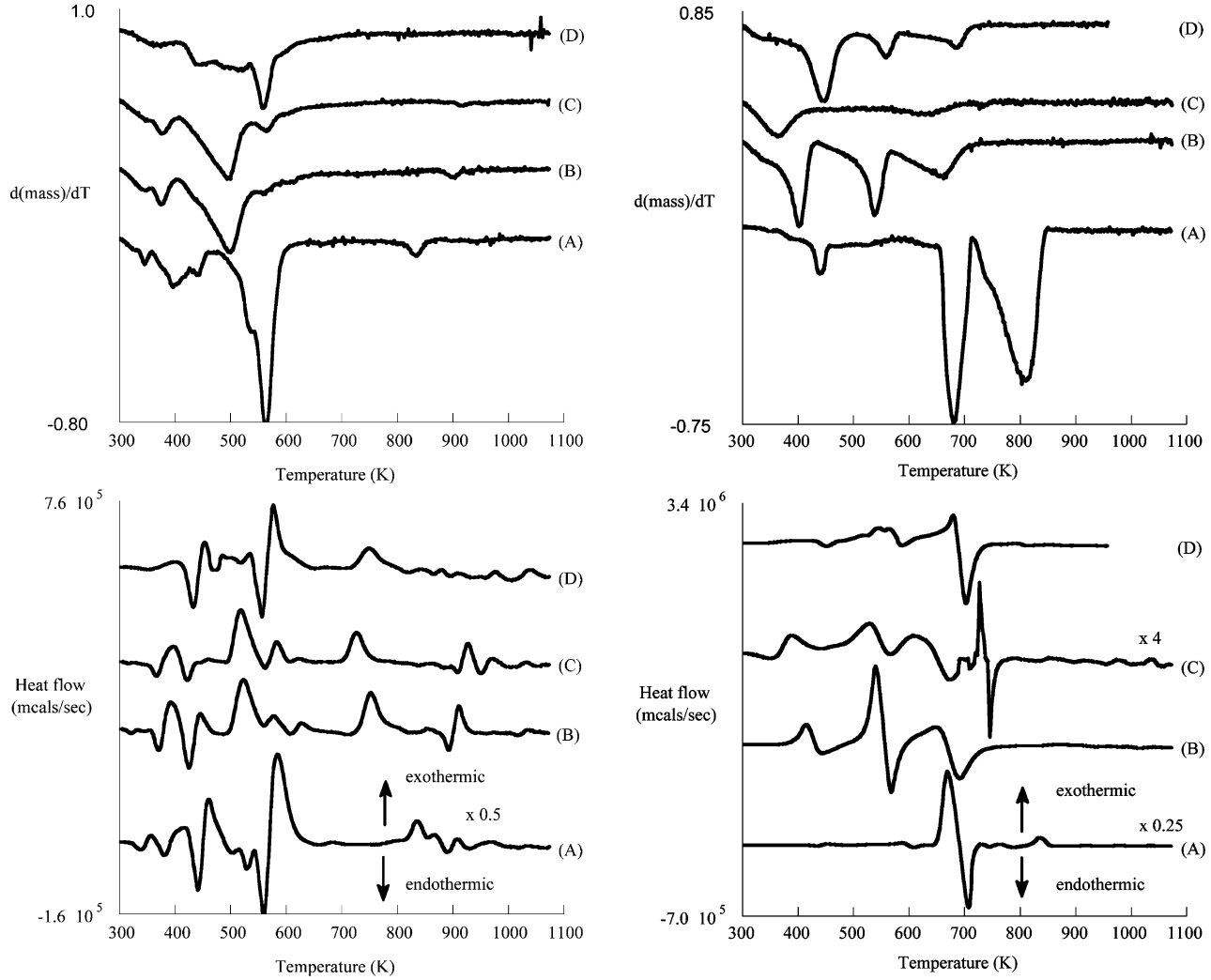

Figure 10. (a, left two panels) TGA (top panel) and DTA (bottom panel) data derived during in situ calcination of uranyl nitrate and of supported (30 wt % U) systems: (A) bulk uranyl nitrate; (B) uranyl nitrate/Al_2O_3; (C) uranyl nitrate/SiO_2; (D) uranyl nitrate/H_1SiO_2. (b, right two panels) TGA (top panel) and DTA (bottom panel) data derived during in situ calcination of UCl_4 and from supported (30 wt % U) systems: (A) bulk UCl_4; (B) UCl_4/Al_2O_3; (C) UCl_4/SiO_2; (D) UCl_4/H_1SiO_2.

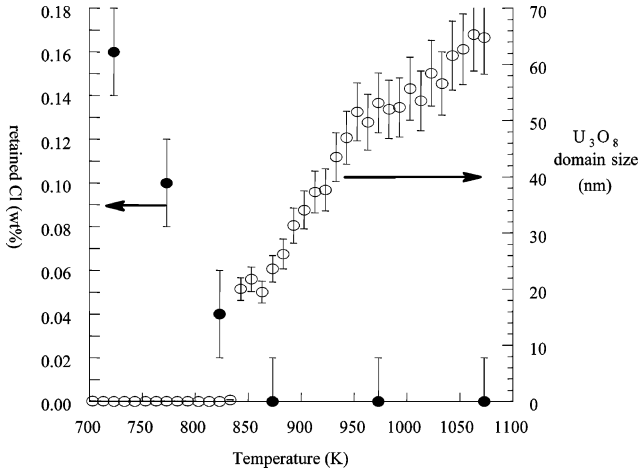

Figure 11. Postcalcination ICP-determined levels of Cl retention, and in situ PXRD-derived U_3O_8 crystallite sizes, during calcination in air, at a range of temperatures for the $U^{IV}Cl_4/\gamma$-Al_2O_3 system.

surface area and pore size distribution measurement, this gradually decreases with increasing calcination temperature to a value of ca. 1 OH nm^{-2} at 1000 K. Thereafter rapid dehydroxylation is observed.

In the absence of other factors, however, these measurements show that calcination of the H_1SiO_2 support materials will not in itself result in a total collapse of the mesoporous architecture even at the highest calcination temperatures applied to the uranium-deposited catalysts (1073 K) over a period of 16 h.

Deposition of uranyl nitrate hexahydrate, followed by drying leads, in all cases investigated to the formation of a supported dihydrate. The observation of a dihydrate form of the uranium phase is consistent with the available literature concerning the thermal decomposition of $U(O)_2(NO_3)_2 \cdot 6H_2O$,[28] wherein two dehydration events occur at ~333−363 and 363−373 K, leading to the formation of a dihydrate: in this respect at least, supporting this precursor does not seem to have perturbed the behavior of the supported species significantly.

The deposition of UCl_4, however, leads to a much more complex supported uranium phase for which no direct analogue can be found through reference to the literature. Further, the local coordination of the U atom, as evidenced by U L_{III} EXAFS, cannot be described in terms of that expected from bulk UCl_4, the closest match being that due to an orthorhombic $UOCl_2$ type species.[21]

The fitting of U−U scatterers at the relatively short distances of 3.68 and 4.31 Å, in tandem with the U−Cl and U−O

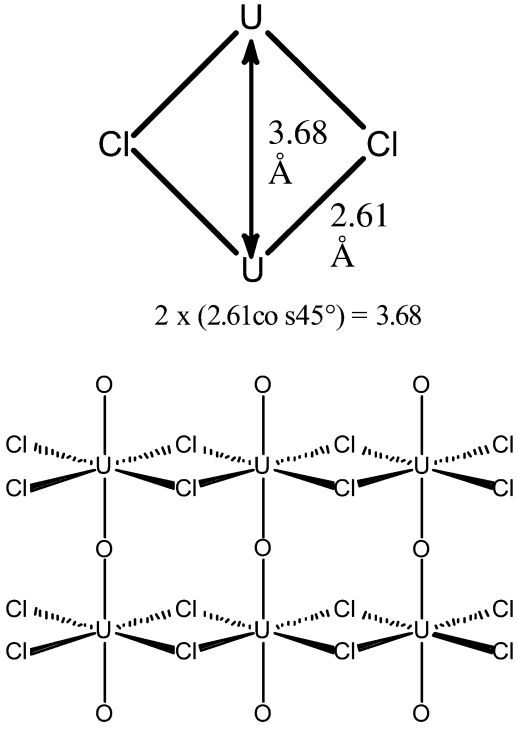

Figure 12. (a, top) Illustration of the origin of multiple scattering pathways arising in U L_{III} edge EXAFS studies of the dried 30 wt % uranium, UCl_4/H_1SiO_2 system. (b, bottom) Structural description of the species formed through deposition of UCl_4 in tetrahydrofuran to Brij76-templated H_1SiO_2 and subsequent drying at 373 K based upon in U L_{III} edge EXAFS data. It should be pointed out that the axial U−O−U bond angles are not actually linear and that the axial linkage of alternate $U(O)_2Cl_2$ units will be staggered slightly in and out of the plane of the page.

distances fitted, indicate the presence of bridging U−Cl−U and slightly nonlinear U−O−U bonding, as shown in Figure 12a. Taken in sum the EXAFS data would seem to indicate the formation of a uranium oxychloride phase of the type shown in Figure 12b. Again, similar results were obtained from all the supports investigated, indicating that the nature of the dispersant has little influence on the phase of uranium initially deposited.

The influence of the supports does, however, manifest itself in the thermal decomposition of the adsorbed uranium precursors and the subsequent formation of U_3O_8 from them. Supporting these precursors generally results in the promotion of the initial precursor decomposition (the exception being the uranyl nitrate precursor supported on the most hydrophobic support, i.e., H_1SiO_2). This promotion of precursor decomposition is most considerable in the UCl_4-derived systems. Uranium tetrachloride and its oxychlorides are, in their own right, very moisture-sensitive, and our observations would seem to imply that moisture not removed by low-temperature drying and/or surface hydroxyl groups may actively participate in promoting decomposition.

It is clear also from both in situ diffraction measurements and TGA/DTS that the adsorbed precursors decompose initially to yield a poorly ordered, essentially nondiffracting phase. The onset of "PXRD visible" U_3O_8 formation shows only a small dependence upon the precursor. Cl-containing systems promote the formation of XRD visible U_3O_8 on H_1SiO_2 and Al_2O_3 supports such that at 743 K they are the only systems which show U_3O_8 domains in PXRD. More detailed investigation however shows that this promoting effect is relatively small (<50 K between chlorinated and nonchlorinated systems supported upon H_1SiO_2).

More considerable, are the observed variations in the appearance of U_3O_8 in XRD as a function of support, with a 110−160 K differential in the onset of the formation of this phase observed between mesoporous and amorphous silicas. These differentials appear to further result in a wide-ranging variation in the net U_3O_8 particle thickness produced by calcination to 1073 K. Indeed, the low-temperature onset of U_3O_8 in the mesoporous systems results in massive U_3O_8 domains compared to both amorphous supports and the intrinsic pore sizes of the H_1SiO_2 itself.

The formation of these extremely large domains of orthorhombic U_3O_8 points to the induction of a large-scale extrusion of this phase from the mesopores by calcination at 1073 K. What is, however, clear is that this occurs with little or no more loss of structural integrity in the support. Indeed, compared to an unloaded H_1SiO_2 calcined in the same manner, the pore size distribution derived from the uranium nitrate-loaded samples after calcination to 1073 K is practically identical to that derived from the unloaded support treated in the same manner.

Conclusions

The use of a Brij 76 templating agent results in highly ordered, thermally stable, H_1SiO_2 materials. The materials show a net 30% loss of total surface area upon calcination in air to ca. 1000 K, and a progressive shrinkage of average pore size from ca. 38 to 30 Å is observed. Above 1100 K a rapid collapse of the mesoporous architecture is evident with concurrent drastic losses in surface area.

Titration of the accessible surface hydroxyl concentrations shown by the H_1SiO_2 support indicate that these materials are more hydrophobic than their amorphous counterparts, showing, at best, surface OH concentrations which are ca. 50% of that obtainable on amorphous silicas. Total dehydroxylation of these materials occurs by 1200 K.

Uranyl nitrate hexahydrate deposition to H_1SiO_2, amorphous SiO_2, and γ-Al_2O_3 leads to the formation of an analogous dihydrate upon drying. The deposition of $U^{IV}Cl_4$, however, leads to the formation of a new supported $UOCl_2$ phase.

Supporting the uranium precursors leads to promotion of their decomposition (especially in the chlorinated cases) save for the case of the uranyl nitrate adsorbed upon the mesoporous support. All precursors collapse to yield an amorphous, nondiffracting phase at temperatures less than 600 K

The formation of the supported uranium phase nominally active for the catalytic reduction of NO by CO, and the oxidation of CO (U_3O_8) by O_2, is shown to have a variety of dependencies both on the precursor and support used but in no case is seen to evolve at a temperature less than 730 K.

It has been found that a small promotion in the evolution of U_3O_8 is observed when starting from the $UOCl_2$ phase compared to the supported uranyl nitrate dihydrate when supported upon mesoporous silicas or amorphous Al_2O_3, but not amorphous SiO_2. However, this is significantly outweighed by pronounced variations in the onset of U_3O_8 formation according to the support used. The use of the mesoporous support significantly promotes the formation of this phase compared to both amorphous SiO_2, and γ-Al_2O_3 dispersants and apparently modifies the manner of its genesis: it is only in the mesoporous cases that a clearly hexagonal phase is seen to develop first before being replaced by the orthorhombic. Subsequently much larger domains of U_3O_8 for equivalent treatment are formed on the mesoporous support compared to the amorphous cases.

The size of the U_3O_8 domains formed after calcination to 1073 K is indicative of a large-scale extrusion of the supported phase from the mesopores due to this treatment. Surface area and pore size distribution measurements however indicate that the mesoporous nature of this support has been largely retained during this process.

Acknowledgment. BNFL and the EPSRC are thanked for funding a Ph.D. studentship to T.C., and the EPSRC are thanked for postdoctoral funding to M.A.N. We thank the director of CCLRC for access to facilities and Dr. Fred Mosselmans for assistance in obtaining XAFS data.

References and Notes

(1) For instance, Bagnall, K. W. In *Lanthanides and Actinides*; Bagnall, K. W., Ed.; Butterworth: London, 1972.

(2) Corberan, V.; Corma, A.; Kremenic, G. *Ind. Eng. Chem. Prod. Res. Dev.* **1984**, *24*, 546; **1985**, *24*, 62.

(3) Callahan, J. L.; Gertissier, B. U.S. Patent 3,308,151, 1967. Callahan, J. L.; Gertissier, B. U.S. Patent 3,198,750, 1965.

(4) Steenhof de Jong, J. C.; Guffens, C. H. E.; Van der Baan, H. F. S. *J. Catal.* **1972**, *26*, 401; **1973**, *31*, 127.

(5) Collette, H.; Deremince-Mathieu, V.; Gabelica, Z.; Nagy, J. B.; Derouane, E. G.; Verbist, J. J. *J. Chem. Soc., Faraday Trans.* **1987**, *83*, 1263.

(6) Hutchings, G. S.; Heneghan, C. S.; Hudson, I. D.; Taylor, S. H. *Nature* **1996**, *384*, 341.

(7) Nozaki, F.; Ohki, K. *Bull. Chem. Soc. Jpn.* **1972**, *45*, 3473.

(8) Nozaki, F.; Kobayashi, M.; Yoshida, S. *Nippon Kagaku Kaishi* **1972**, 26.

(9) Nozaki, F.; Matsukawa, F.; Mano, Y. *Bull. Chem. Soc. Jpn.* **1975**, *48*, 2674.

(10) Collette, H.; Maroie, S.; Riga, J.; Verbist, J. J.; Gabelica, Z.; Nagy, J. B.; Derouane, E. G. *J. Catal.* **1986**, *98*, 326.

(11) Pollington, S. D.; Lee, A. F.; Overton, T. L.; Sears, P. J.; Wells, P. B.; Hawley, S. E.; Hudson, I. D.; Lee, D. F.; Ruddick, V. *Chem. Commun.* **1999**, 725.

(12) Attard, G. S.; Glyde, J. C.; Göltner, C. G. *Nature* **1995**, *378*, 366.

(13) Dollimore, D.; Heal, G. R. *J. Appl. Chem.* **1964**, 109.

(14) Herman, J. A.; Shuttle, J. F. *Inorg. Synth.* **1957**, *5*, 143.

(15) Schleid, T.; Meyer, G.; Morss, L. R. *J. Less. Common Met.* **1987**, *69*, 132.

(16) Krupa, J. C. *Inorg. Chim. Acta* **1987**, *139*, 223.

(17) Taylor, J. C.; Wilson, P. W. *Acta Crystallogr.* **1973**, *29*, 1942.

(18) Binsted, N. *PAXAS: Programme for the Analysis of X-ray Absorption Spectra*; University of Southampton: Southampton, U.K., 1988.

(19) Binsted, N. EXCURV98, CCLRC Daresbury Laboratory computer programme, 1998.

(20) Turin, S. Ph.D. Thesis, University of Southampton, U.K., 2000.

(21) Dalley, N. K.; Mueller, M. H.; Simonsen, S. H. *Inorg. Chem.* **1971**, *10*, 323.

(22) Taylor, J. C.; Wilson, P. W. *Acta Crystallogr., Sect. B: Struct. Crystallogr. Cryst. Chem.* **1974**, *30*, 175.

(23) Roussel, P. B.; Hitchcock, P. B.; Tinker, N. D.; Scott, P. *Inorg. Chem.* **1997**, *36*, 5716.

(24) Burns, P. C.; Ewing, R. C.; Hawthorne, F. C.; *Can. Mineral.* **1997**, *35*, 1551.

(25) Van Der Sluys, W. G.; Berg, J. M.; Barnhardt, D.; Sauer, N. N. *Inorg. Chim. Acta* **1992**, *204*, 251.

(26) Scherrer, P. *Nachr. Göttinger Gessell.* **1918**, 98.

(27) Hoekstra, H. R.; Siegel, S.; Gallagher, F. X. *J. Inorg. Nucl. Chem.* **1970**, *32*, 3237.

(28) Dash, S.; Kamruddin, M.; Bera, S.; Ajikumar, P. K.; Tyagi, A. K.; Narasimhan, S. V.; Raj, B. *J. Inorg. Nucl. Chem.* **1999**, *264*, 271.

(29) Cordefunke, E. H. P. *J. Inorg. Nucl. Chem.* **1977**, *39*, 2189.